Electronic Supplementary Information (ESI)

for

The effect of functional groups on the glass transition temperature of atmospheric organic compounds: A molecular dynamics study

Panagiota Siachouli,[a,b] Katerina S. Karadima,[a,b] Vlasis G. Mavrantzas,*,[a,b,c] and Spyros N. Pandis*,[a,b]

[a]Department of Chemical Engineering, University of Patras, Patras, 26504, Greece

[b]Institute of Chemical Engineering Sciences (ICE–HT/FORTH), Patras, 26504, Greece

[c]Particle Technology Laboratory, Department of Mechanical and Process Engineering, ETH Zürich, CH-8092 Zürich, Switzerland

S1. Force-field evaluation

Validation tests were carried out in order to evaluate the force field utilized in this study. First we compared the utilized force field (LigParGen OPLS) to L-OPLS[2,3] for the case of *1*-hexanol. As it can be seen in Table S1, the L-OPLS estimates of the T_g are on average within the regime (albeit slightly higher) of the LigParGen OPLS ones. Note that the experimental T_g is reported to be (averaged) 134 ± 11 K [4] and thus LigParGen OPLS, employed in this article, predicts a T_g closer to the experimental one.

Table S1: Comparison of LigParGen OPLS-AA and L-OPLS force fields for the case of 1-hexanol.

No of configuration	T_g (K) from the LigParGen OPLS (using the temperature variation of density/non-bonded potential energy of interaction)		T_g (K) from L-OPLS (using the temperature variation of density/non-bonded potential energy of interaction)	
1	144.6	146.8	151.7	145.6
2	144.5	145.2	162.8	159.7
3	159.8	160.1	163.9	162.7
Average	149.6	150.7	159.4	156

Next, we chose to compare the MD-predicted densities to the experimental ones. Most of the experimental densities are reported at around 300 K, thus we restricted the comparison only among the compounds whose melting point is below 300 K. The list included: *1*-propanol, *2*-propanol, *1,2*-propanediol, *1,3*-propanediol, *1,2,3*-propanetriol, *1*-hexanol, *1,6*-hexanediol, propionic acid and hexanoic acid. As can be seen in Fig. S1, the agreement between experimental and MD-predicted densities is striking. For most of the compounds, the maximum deviation is less than 1% and only *1,2,3*-propanetriol shows a 4.4% deviation from the reported experimental density. Note that the melting point of *1,2,3*-propanetriol is very close to 300 K, which could partly explain its "higher" deviation compared to the rest of the compounds.
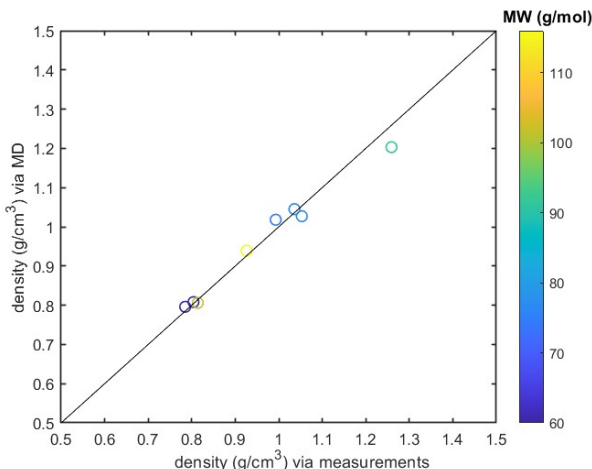
Figure S1: Comparison of experimental densities versus MD-predicted ones as a function of the molecular weight. The compounds depicted are: 1-propanol, 2-propanol, 1,2-propanediol, 1,3-propanediol, 1,2,3-propanetriol, 1-hexanol, 1,6-hexanediol, propionic acid and hexanoic acid. The solid line is the 1:1 line.

S2. Example calculation of T_g

To illustrate our method, we use as an example the determination of T_g for MBTCA. The curve of density as a function of temperature is depicted in Figure S2 . Each point in the curve represents the system at a specific temperature and density, the cooling step implemented here is starting at 410 K and using a cooling step of 20 K per 2 ns. The density increases as the temperature decreases and a slope change occurs at 331 K, corresponding to the estimated T_g. The non-bonded energy shows a slope change at 338 K. The T_g values examining the properties are in a good agreement differing only by ~ 7 K. These values are also in a good agreement with the T_g determination implementing the segmental relaxation methodology than be found in Section 3.2.3 of the main article. However, note that this differs with experimental values which report T_g values in the (300-305) K range for MBTCA.[1]
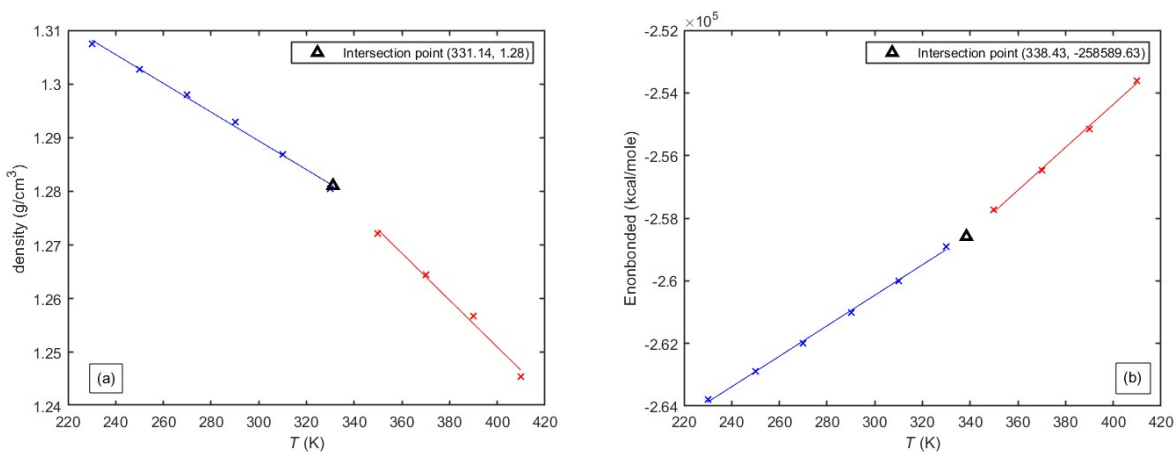

Figure S2: Estimation of T_g for MBTCA via: (a) density and (b) non-bonded energy.

S3. Fitting selection

 The determination of the bilinear fit is done by first detecting at which point of the property of interest the mean value changes most significantly. In the following example (Fig. S3) we see the density of MBTCA as a function of temperature. The changing point is the data in point 7 which corresponds to the temperature of 330 K. We split the set of our 10 data points in three possible bilinear fits as follows: (a) 1-6 and 7-10, (b) 1-5 and 6-10 and (c) 1-7 and 8-10. The bilinear fit chosen is eventually

the one depicted in Fig. S3a. The reasoning is to find around the point with the most significant change in the density/non-bonded interactions the optimal combination of R^2. As an overall strategy we split in two and add/subtract one point from the one fit to the other and examine the R^2 pairs.
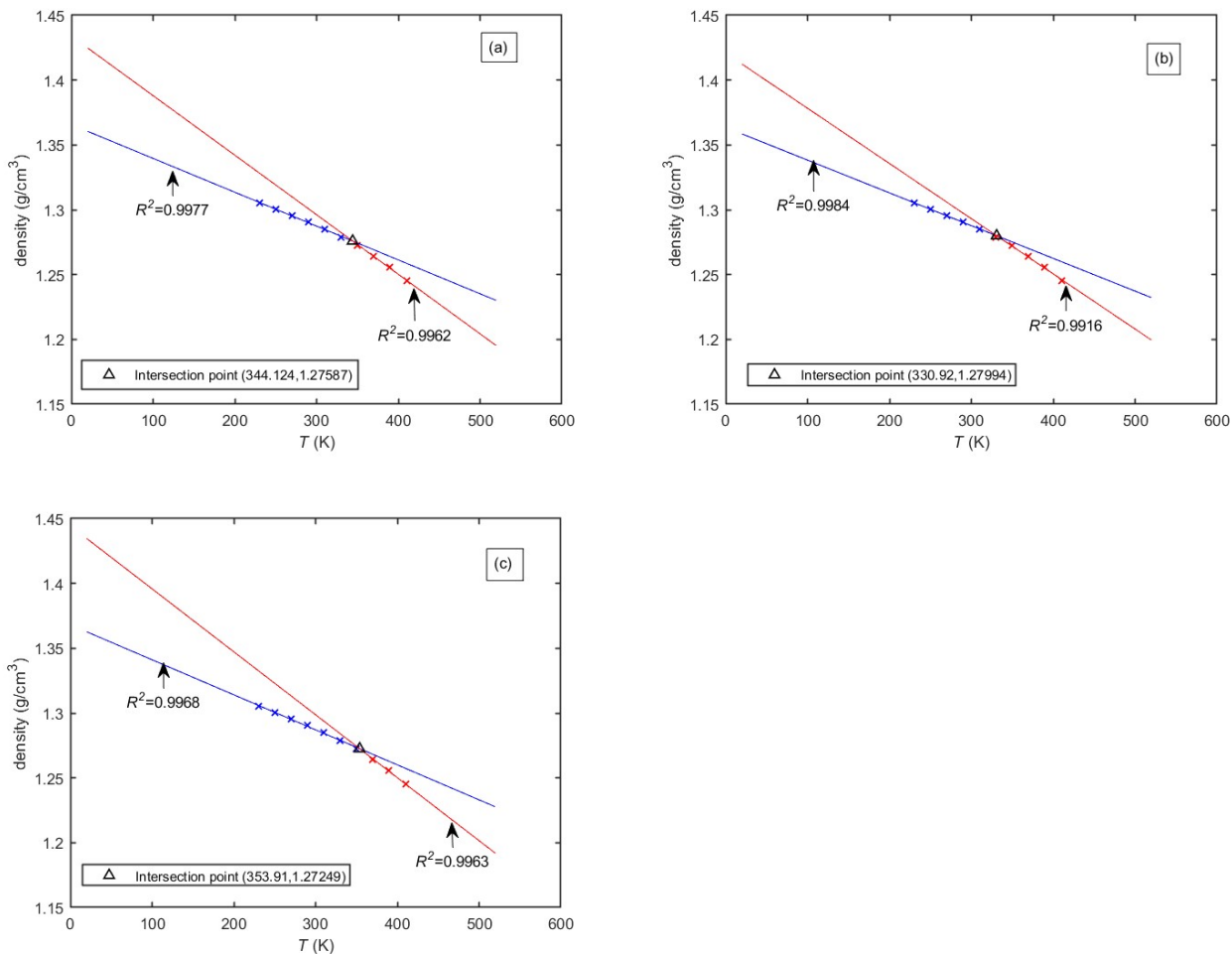

Figure S3: Detection of the optimal bilinear fit protocol. Part (a) of the Figure shows the optimal bilinear fit whereas Parts (b) and (c) show the rejected bilinear fits that were considered.

S4. Effect of cooling step

We present here as an example the case of MBTCA. For each cooling step, three independent initial configurations were used for the prediction of T_g. The highest T_g predictions were obtained for the lowest cooling step (Table S2). The higher cooling step is closer to the reported experimental values of MBTCA, which are in the (300-305) K range[5] and also in better agreement with the segmental relaxation method implemented for MBTCA and CPA depicted in Section 3.2.3.

Table S2: The effect of cooling step on T_g. Comparison of T_g predictions for 5K per 2ns, 10K per 2ns, 20K per 2ns and 30K per 2ns for MBTCA organic compound. A sample of three independent initial configurations was used for the four different cooling steps.

No of configurations	Predicted T_g (K)

	5K per 2ns (from the temperature variation of density/non-bonded potential energy of interaction)		10K per 2ns (from the temperature variation of density/non-bonded potential energy of interaction)		20K per 2ns (from the temperature variation of density/non-bonded potential energy of interaction)		30K per 2ns (from the temperature variation of density/non-bonded potential energy of interaction)	
1	356	355.9	364.6	356.8	344.1	358.3	344.3	346.6
2	359.3	355.1	344.8	346.8	331.1	338.4	337.4	344
3	352.1	357.2	350.2	349.7	341.2	357.1	346.6	352.1
Average	355.8±3.6	356±1.05	353.2±10.2	351.1±5.1	338.7±6.7	351.2±11.1	342.7±4.7	347.5±4.1

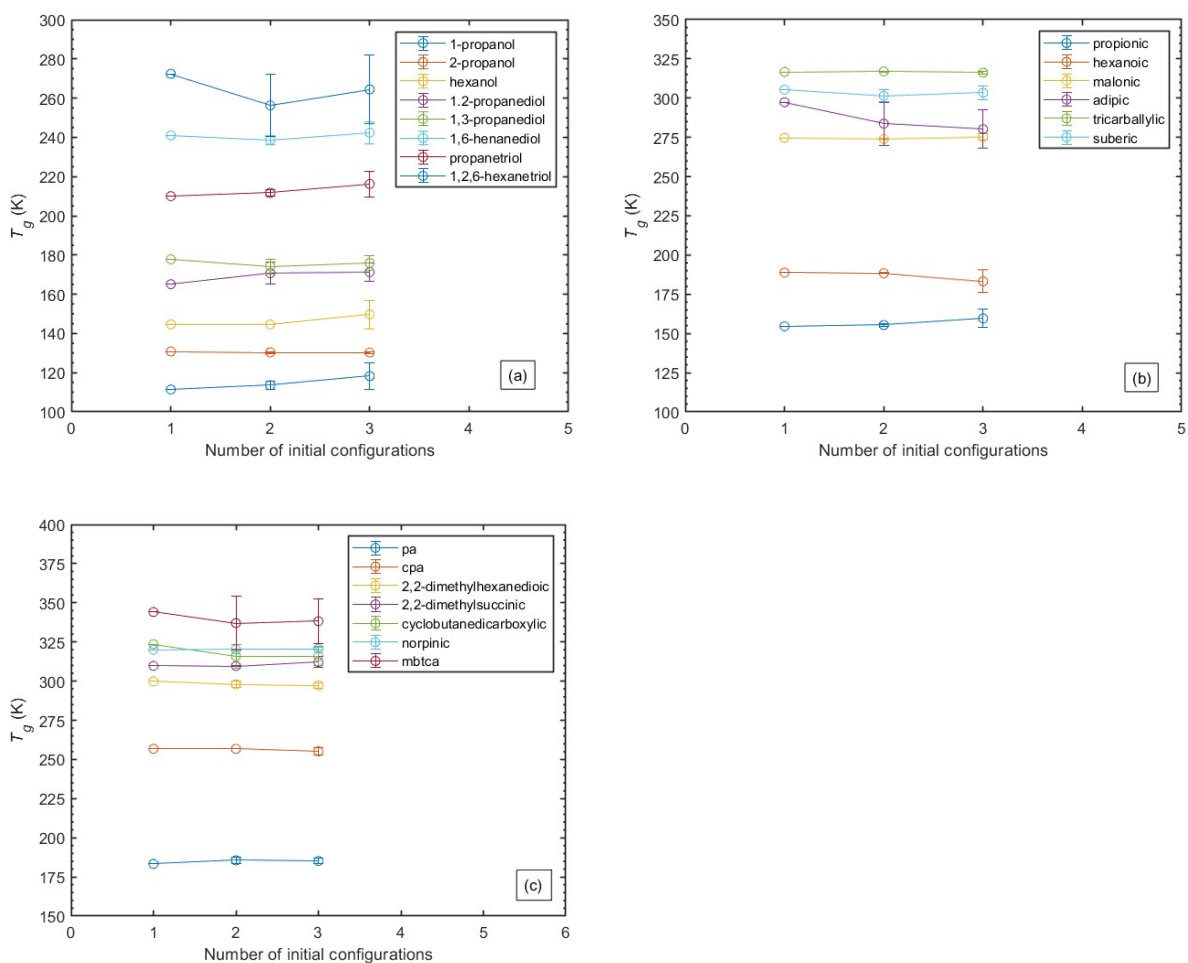## S5. Dependency on initial configuration

Figure S4: The evolution of T_g with the addition of different initial configurations. Part (a) depicts the linear alcohols, Part (b) the linear acids, and Part (c) the non-linearly structured compounds.

S6. Comparison of MD with other approaches

For most of the compounds investigated in this work, there exist no experimental measurements to compare against our MD predictions for a more detailed validation of our work. Therefore, the Boyer-Kauzmann rule has been a guide to our work as well as some melting points that were obtained from online databases or handbooks. We report some of them in Table S3 below.

Table S3: Melting point of organic compounds from various References.

Compound	Melting point temperature (K)	Reference
_1_-Propanol	146	Beaman (1952)[6]
_1_-Propanol	147.15	Jean-Claude Bradley Open melting point dataset[7]
_2_-Propanol	183.99	Chemspider (EPISuite)[8]
_1,2_-Propanediol	240.15	Chemspider (EPISuite)[9]
_1,3_-Propanediol	246.15	Jean-Claude Bradley Open melting point dataset[7]
_1,2,3_-Propanetriol	291.15	Beaman (1952)[6]
_1_-hexanol	228.55	C.L. Yaws (2007)[10]
_1,6_-hexanediol	315	Chemspider[11]
_1,2,6_-hexanetriol	324.15	Chemspider[12]
Propionic acid	252.15	PubChem[13]
Hexanoic acid	270	Chemspider[14]
Malonic acid	408.15	Chemspider[15]
Adipic acid	425	Chemspider[16]
Suberic acid	417.15	Chemspider[17]
Tricarballylic acid	434	Chemspider[18]
Cis-pinonic acid	377	A.Kołodziejczyk et al. (2019)[19]
Pinonaldehyde	324	Chemeo[20]
3-Methyl-_1,2,3_-butanetricarboxylic acid	417	A.Kołodziejczyk et al. (2020)[5]
_2,2_-Dimethylsuccinic acid	413.65	Pubchem[21]
_2,2_-Dimethylhexanedioic acid	387.15	Chemspider[22]
Cyclobutanedicarboxylic acid	431.15	Chemspider[23]
Norpinic acid	440.68	A.Kołodziejczyk et al. (2019)[19]

S7. The effect of O:C and molecular weight
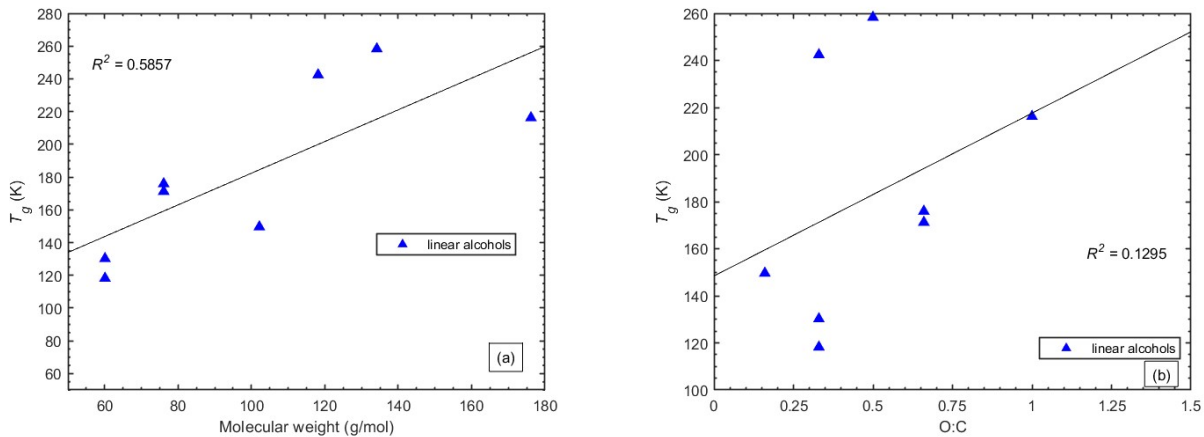
S7.1 Linear alcohols

Figure S5: The T_g of linear alcohols as a function of (a) molecular weight and (b) O:C ratio.
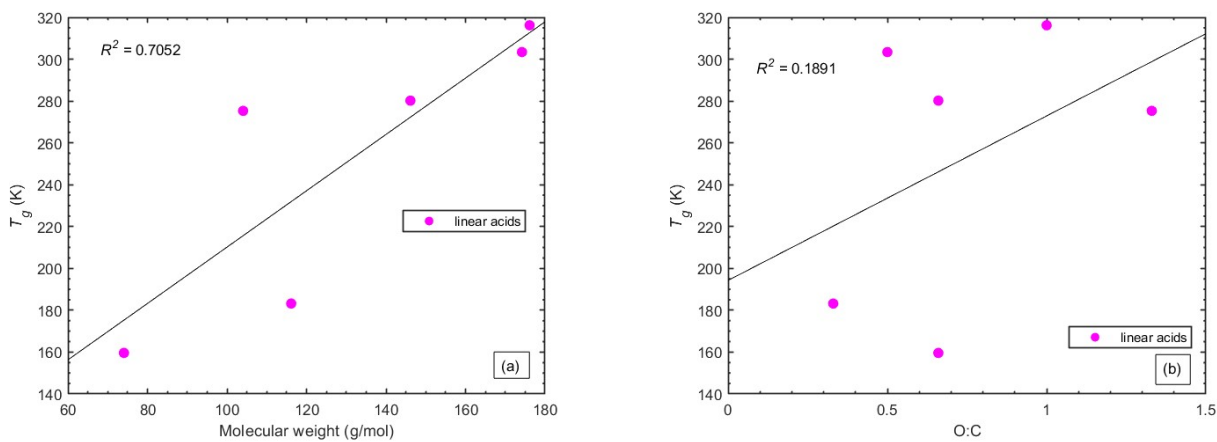
S7.2 Linear acids

Figure S6: The T_g of linear acids as a function of (a) molecular weight and (b) O:C ratio.
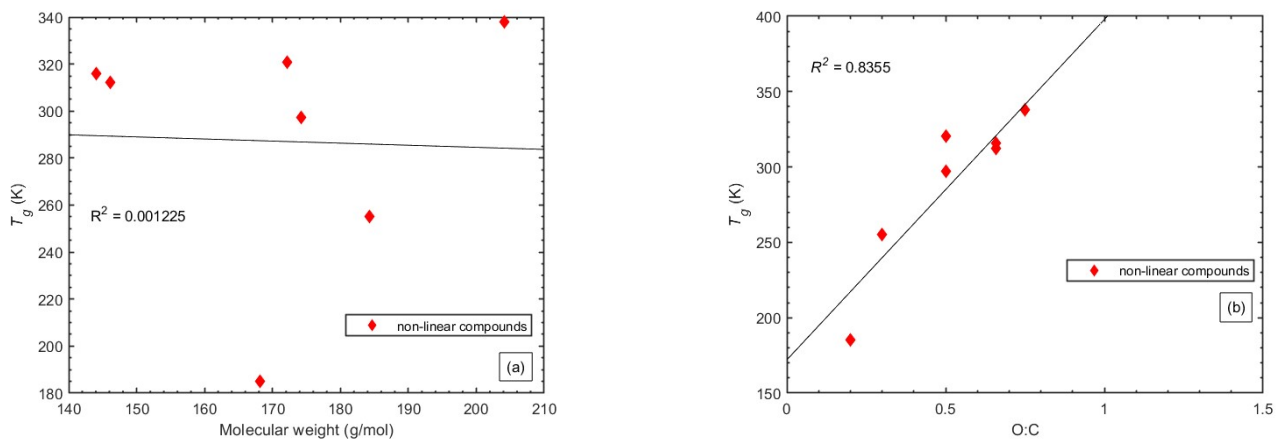
S7.3 Non-linear compounds

Figure S7: *The T_g of non-linear compounds as a function of (a) molecular weight and (b) O:C ratio.*

References

1   H. P. Dette, M. Qi, D. C. Schröder, A. Godt and T. Koop, *J. Phys. Chem. A*, 2014, **118**, 7024–7033.

2   S. W. I. Siu, K. Pluhackova and R. A. Böckmann, *J. Chem. Theory Comput.*, 2012, **8**, 1459–1470.

3   K. Pluhackova, H. Morhenn, L. Lautner, W. Lohstroh, K. S. Nemkovski, T. Unruh and R. A. Böckmann, *J. Phys. Chem. B*, 2015, **119**, 15287–15299.

4   N. E. Rothfuss and M. D. Petters, *Environ. Sci. Technol.*, 2017, **51**, 271–279.

5   A. Kołodziejczyk, P. Pyrcz, K. Błaziak, A. Pobudkowska, K. Sarang and R. Szmigielski, *ACS Omega*, 2020, **5**, 7919–7927.

6   R. G. Beaman, *J. Polym. Sci.*, 1952, **9**, 470–472.

7   Jean-Claude Bradley Open Melting point Dataset, https://figshare.com/articles/dataset/Jean_Claude_Bradley_Open_Melting_Point_Datset/1031637, (accessed 15 December 2022).

8   Chemspider, http://www.chemspider.com/Chemical-Structure.3644.html?rid=1fe9f349-2a30-4706-a58e-741a4b9679f1, (accessed 28 November 2023).

9   Chemspider, http://www.chemspider.com/Chemical-Structure.13835224.html?rid=8c397256-a5b5-4aa6-8e7d-2d6b8d3a57a7&page_num=0, (accessed 28 November 2023).

10   C. L. Yaws, *Yaws Handbook of Thermodynamic Properties for Hydrocarbons and Chemicals*, Gulf Publishing Company, first edit., 2007.

11   Chemspider, https://www.chemspider.com/Chemical-Structure.13839416.html?rid=45c7e784-b349-4095-806d-88893666873b, (accessed 20 November 2022).

12   Chemspider, https://www.chemspider.com/Chemical-Structure.7535.html?rid=3d7b8337-f7ab-4ddf-b187-92f038d087a8, (accessed 10 November 2022).

13   PubChem, https://pubchem.ncbi.nlm.nih.gov/compound/Propionic-acid#section=Melting-Point%0A, (accessed 1 May 2023).

14   Chemspider, http://www.chemspider.com/Chemical-Structure.8552.html?rid=191d06bb-181e-4610-8d0f-9f614e1b3192%0A, (accessed 1 May 2023).

15   Chemspider, http://www.chemspider.com/Chemical-Structure.844.html?rid=5f49c4fd-a142-45e7-a36d-25bf93280a56%0A, (accessed 1 May 2023).

16   Chemspider, http://www.chemspider.com/Chemical-Structure.191.html%0A, (accessed 1 May 2023).

17   Chemical Book, https://www.chemicalbook.com/ChemicalProductProperty_EN_CB2775043.htm%0A, (accessed 28 November 2023).

18   Chemspider, http://www.chemspider.com/Chemical-Structure.14220.html?rid=80a5217c-580f-4a50-82bb-

0fcdf788cf29%0A, (accessed 28 November 2023).

19   A. Kołodziejczyk, P. Pyrcz, A. Pobudkowska, K. Błaziak and R. Szmigielski, *J. Phys. Chem. B*, 2019, **123**, 8261–8267.

20   Chemeo, https://www.chemeo.com/cid/86-043-9/Pinonaldehyde, (accessed 1 May 2023).

21   PubChem, https://pubchem.ncbi.nlm.nih.gov/compound/2_2-Dimethylsuccinic-acid#section=Experimental-Properties%0A, (accessed 28 November 2023).

22   Chemspider, http://www.chemspider.com/Chemical-Structure.4954310.html%0A, (accessed 28 November 2023).

23   Chemspider, http://www.chemspider.com/Chemical-Structure.2470.html?rid=b0f4ec52-385b-4981-9fd1-7e9bcd1bc321%0A, (accessed 28 November 2023).